

Title Page

Title: Heterotropic Allosteric Modulation of CYP3A4 In Vitro by Progesterone: Evidence for Improvement in Prediction of Time Dependent Inhibition for Macrolides

Authors: Luc R.A. Rougée, Pooja V. Hegde, Kaitlin Shin, Trent L. Abraham, Alec Bell, Stephen D. Hall

Laboratory of Origin: Lilly Research Laboratories; Eli Lilly and Company, Indianapolis, Indiana
(LRAR, PVH, KS, TLA, AB, SDH)

Running Title Page

Running Title: Allosteric Modulation of Macrolide Time-Dependent Inhibition

Address correspondence to: Luc Rougée, Eli Lilly and Company; Indianapolis, Indiana. Tel. 317-651-9135;

Fax: 317-433-6400; Email address: lrougee@lilly.com

Number of Text Pages: 16

Number of Tables: 4

Number of Figures: 4

Number of References: 38

Number of Words in the Abstract: 226

Number of Words in the Introductions: 750

Number of Words in the Discussion: 1588

Abbreviations: 1'-hydroxymidazolam, 1OH-MDZ; 4-hydroxymidazolam, 4OH-MDZ; Cytochrome P450, CYP; Cytochrome P450 3A4, CYP3A4; Human liver microsomes, HLM; irreversible inhibition constant, K_i ; maximum rate of enzyme inactivation, k_{inact} ; metabolic-intermediate complex, MIC; midazolam, MDZ; progesterone, PGS; physiologically-based pharmacokinetics, PBPK; time-dependent inhibition, TDI; Drug-drug interactions, DDI

Abstract (226 words)

Predictions of drug-drug interactions resulting from time-dependent inhibition (TDI) of CYP3A4 have consistently overestimated or mis-predicted (i.e. false positives) the interaction that is observed in vivo. Recent findings demonstrated that the presence of the allosteric modulator progesterone (PGS) in the in vitro assay could alter the in vitro kinetics of CYP3A4 TDI with inhibitors that interact with the heme moiety, such as metabolic-intermediate complex (MIC) forming inhibitors. The impact of the presence of 100 μM PGS on the TDI of molecules in the class of macrolides typically associated with MIC formation was investigated. Presence of PGS resulted in varied responses across the inhibitors tested. The TDI signal was eliminated for five inhibitors, and unaltered in the case of one, fidaxomicin. The remaining molecules erythromycin, clarithromycin, and troleandomycin, were observed to have a decrease in both potency and maximum inactivation rate ranging from 1.7-fold to 6.7-fold. These changes in TDI kinetics led to a >90% decrease in inactivation efficiency. In order to determine in vitro conditions that could reproduce in vivo inhibition, varied concentrations of PGS were incubated with clarithromycin and erythromycin. Resulting in vitro TDI kinetics were incorporated into dynamic physiologically-based pharmacokinetic (PBPK) models to predict clinically observed interactions. The results suggested that a concentration of $\sim 45 \mu\text{M}$ PGS would result in TDI kinetic values that could reproduce in vivo observations and could potentially improve predictions for CYP3A4 TDI.

Significance Statement (62 words)

The impact of the allosteric heterotropic modulator progesterone on the CYP3A4 time-dependent inhibition kinetics was quantified for a set of metabolic-intermediate complex forming mechanism-based inhibitors. We identify the in vitro conditions that optimally predict time-dependent inhibition for in vivo drug-drug interactions through dynamic physiologically-based pharmacokinetic modeling. The optimized assay conditions improve in vitro to in vivo translation and prediction of time-dependent inhibition.

Introduction (750 words)

A priori understanding of CYP3A4 inhibition by new chemical entities remains a cornerstone of drug discovery. In vitro assays using human liver microsomes (HLM) are routinely used to understand the potential extent and kinetic aspects of inhibition. While in vivo predictions of reversible inhibition using HLM in vitro values has been successful, the translation of time-dependent inhibition (TDI) of CYP3A4 often leads to overestimations of the in vivo clinical drug-drug interaction (DDI) or missed predictions (i.e. false positive signals in vitro that do not translate in vivo) (Obach et al., 2006; Obach, Walsky and Venkatakrishnan, 2007; Vieira et al., 2014). Various attempts to address this apparent disconnect have been proposed. Filppula et al. (2019) suggested that the cytosolic unbound inhibitor concentration could improve DDI predictions as it reflects the fraction of inhibitor capable of eliciting inactivation. In vitro HLM TDI data corrected with a hepatocyte-derived, cytosolic bioavailability term were found to improve mechanistic static model predictions when combined with the maximum unbound-inhibitor concentration at steady state for liver and the total enterocytic concentration for gut (Rostami-Hodjegan and Tucker, 2004; Filppula et al., 2019). However, work by Tseng et al. (2021) found that the use of unbound steady state average systemic concentration and average portal vein concentration for the liver and gut respectively in the mechanistic static model improved DDI predictions using standard in vitro HLM TDI data. A suite of models has also been proposed that exploits the non-log linear loss of the activity observed in a replot analysis of some inhibitors. This approach incorporates additional features such as multiple binding kinetics, membrane partitioning, inhibitor depletion, and sequential metabolism in inactivation models when fitting data (Korzekwa et al., 2014; Nagar, Jones and Korzekwa, 2014; Yadav, Korzekwa and Nagar, 2018). These models have proved to provide improved predictability of clinical DDIs for some mechanism-based inhibitors, whilst requiring a priori estimates of key rate constants and generation of additional data necessary for model fitting. Regardless of the approach, the improvements are not ubiquitous, and in some cases does not address false positive signals observed in vitro. Boundaries on the inactivation rates determined in vitro for HLM and hepatocytes have been proposed under which translation of in vitro signals are unlikely to translate to an in vivo DDI observation (Eng et al., 2020). Although this empirically helps to eliminate some of

the false positives, many compounds with in vitro inactivation rates above the boundary do not result in a clinical interaction. Therefore, an understanding of the potential underlying mechanisms for this disconnect is needed. A commonality in these approaches is the assumption that the in vitro-determined HLM TDI values correctly reflect in vivo.

Recent work demonstrated that the interaction of the allosteric modulator progesterone (PGS) with the peripheral allosteric binding site of CYP3A4 influenced the extent of TDI observed on known CYP3A4 mechanism-based inhibitors (MBIs) (Rougée et al., 2023). Presence of PGS changed the TDI kinetics of four known CYP3A4 time-dependent inactivators across different mechanisms. Inhibitors whose mechanisms involved interaction with the heme moiety of the CYP enzyme were most sensitive to the allosteric modulation by PGS. Significant decreases in potency and inactivation rate were observed in the presence of PGS for mibefradil which acts via heme destruction, and clarithromycin and troleandomycin (TAO) which form a metabolic-intermediate complex (MIC). This reduction in formation of the MIC with CYP3A4 by clarithromycin and TAO in the presence of PGS would result in a better alignment with the observed DDIs, suggesting that the absence of allosteric modulation of CYP3A4 may contribute to the poor translation of HLM based DDIs.

The current study examined the impact of allosteric modulation on the TDI measured in HLM and the formation of MIC by macrolide antibiotics. This class of molecules is known to form MICs, although some have not been found to result in clinical DDI (von Rosensteil and Adam, 1995; Westphal, 2000; Fohner et al., 2017). Time-dependent inhibition of nine macrolide molecules azithromycin, clarithromycin, erythromycin, fidaxomicin, roxithromycin, spiramycin, tilmicosin, TAO, and tylosin were investigated in the absence and presence of a concentration of PGS previously shown to impact MBIs. To determine in vitro conditions that reflect in vivo TDI, a range of PGS concentrations were tested on two known MBIs, clarithromycin and erythromycin. In vitro established TDI kinetic values were then incorporated into dynamic physiologically-based pharmacokinetic (PBPK) models to predict DDIs and establish a concentration of PGS in vitro that

recapitulates clinical observations of inhibition to establish in vitro conditions that translate DDI from HLM in drug discovery.

Materials and Methods

Materials. Chemical reagents were obtained commercially: 1'-OH midazolam, 1'-OH midazolam-d4 (Cerilliant Corp, Round Rock, Texas); progesterone, sodium phosphate monobasic, sodium phosphate dibasic, phosphoric acid, sodium hydroxide (Fisher Scientific, Pittsburgh, PA); β -Nicotinamide adenine dinucleotide 2'-phosphate reduced tetrasodium salt hydrate (NADPH), midazolam, 4-hydroxymidazolam, clarithromycin (Sigma Aldrich, St. Louis, MO), erythromycin (ApexBio, Houston, TX), troleandomycin (Abcam, Cambridge, MA), Azithromycin (Selleckchem, Houston, TX), fidaxomicin (MedChem Express, Monmouth Junction, NJ), roxithromycin (Crescent Chemical, Islandia, NY), spiramycin (Sigma Aldrich, St. Louis, MO), tilmicosin (Sigma Aldrich, St. Louis, MO), tylosin (Sigma Aldrich, St. Louis, MO). Recombinant CYP Supersomes® (rCYP) and pooled human liver microsomes (HLM) (150 individuals, equal proportion male and female, UltraPool™®, Lot. #38291) were purchased from Corning (Woburn, MA).

Time-Dependent Inhibition (K_I and k_{inact} Determination). The first order maximum inactivation rate constant (k_{inact}) and irreversible inhibition constant (K_I) were determined using the dilution method (Mohutsky and Hall, 2014) as previously described (Rougée et al., 2023). Briefly, azithromycin (0-250 μ M), clarithromycin (0-100 μ M), erythromycin (0-100 μ M), fidaxomicin (0-250 μ M), roxithromycin (0-200 μ M), spiramycin (0-250 μ M), tilmicosin (0-250 μ M), troleandomycin (0-10 μ M), or tylosin (0-250 μ M) was incubated at 37°C with pooled HLM (0.5 mg/ml) and NADPH (1 mM) in 100 mM Na_2HPO_4 buffer at pH 7.4 for 0, 2.5, 6, 15, 30, 45, and 60 minutes. After pre-incubation, a 20-fold dilution into a secondary incubation containing 30 μ M midazolam (MDZ) with NADPH (1 mM) was performed. The secondary incubation was allowed to proceed for 2 minutes at 37°C, after which an aliquot (50 μ l) was added to 100 μ l of 50:50 (v/v) MeOH:ACN containing internal standard to stop the reaction. Plates were sealed with Easy Pierce 20 mm foil

(Thermo Fisher Scientific), vortexed for 20 second, centrifuged (3500g for 10 minutes) and analyzed by LC-MS/MS for the formation of 1'-hydroxymidazolam (1OH-MDZ) and 4-hydroxymidazolam (4OH-MDZ).

The assay was performed under the following conditions for all inhibitors: 1) Solvent control in primary incubation with allosteric modulator PGS 5 μ M in the secondary reaction (final concentration). Concentration reflects the final concentration after 20-fold dilution of the top concentration of PGS tested in the primary incubation; 2) Allosteric modulator PGS 100 μ M in primary incubation. Secondary incubations all contained a final concentration of PGS 5 μ M after dilution.

Finally, a screen with varying concentrations of PGS was performed for clarithromycin and erythromycin as the perpetrators. The assay was performed with concentrations of 0, 1, 10, 20, 40, 60, 80 and 100 μ M PGS in the primary incubation. The concentration of PGS in the secondary reaction was adjusted in the lower concentrations to achieve the same final concentration of allosteric modulator as the highest concentration after the dilution step. That is, the secondary incubations all contained a final concentration of 5 μ M PGS.

Metabolic-Intermediate Complex Formation. Monitoring of the formation of the MIC was performed as follows. A sample cuvette containing 200 pmol human recombinant CYP3A4 (+ P450 Reductase + Cytochrome b₅) in 100 mM Na₂HPO₄ buffer pH 7.4, perpetrator (clarithromycin 100 μ M; troleandomycin 10 μ M, erythromycin 100 μ M, azithromycin 250 μ M, spiramycin 250 μ M, tilmicosin 250 μ M, roxithromycin 200 μ M, fidaxomicin 250 μ M, tylosin 250 μ M) in 0.9%:0.1% (v/v) MeOH:DMSO, and either MeOH or 100 μ M PGS in MeOH, and a reference cuvette containing the same as the sample cuvette with the exception that the perpetrator was replaced with solvent 0.9%:0.1% (v/v) MeOH:DMSO alone were prepared. After incubating for 5 mins at 37°C, NADPH (1 mM final concentration) was added to bring final volume to 1 mL, reactions were mixed through inversion, and difference spectra from 400-500 nm were taken using a Lambda 365 dual beam spectrophotometer with a Peltier controlled fluid circulator to maintain cuvette temperature at 37°C (Perkin Elmer, Waltham, MA). Cuvettes were not stirred. Scans were performed at 5-min intervals up to 30 mins. Absorbance at 490 nm was subtracted from the resulting data points and plotted. The amount of CYP MIC

formed over time was quantitated using the extinction coefficient $65 \text{ mM}^{-1} \text{ cm}^{-1}$ (Pershing and Franklin, 1982) and the difference between absorbance maxima (455 nm) and 490 nm ($\Delta A_{455-490}$).

LC-MS Analysis. Samples were analyzed by LC-MS/MS using the quadrupole function on a Sciex (Framingham, MA) QTrap 6500+ mass spectrometer equipped with a TurboIonSpray interface and operated in positive ion mode. The pumps were Shimadzu (Kyoto, Japan) LC-40D x3 units with a CBM-40 controller, and a CTC (Zwingen, Switzerland) PAL RSI liquid handler was used as the autosampler. Separation of 1OH-MDZ and 4OH-MDZ was accomplished using a Waters Acquity BEH C18 2.1 x 50mm 1.7 micron column with a column heater setting of 40°C. Water:Formic Acid 1000:1 (v/v) comprised Mobile Phase A, ACN:Formic Acid 1000:1 (v/v) comprised Mobile Phase B. Analytes were monitored by MRM using Q1/Q3 transitions of m/z 342.1/203.1 (collision energy 40) and 342.1/234.1 (collision energy 33) for 1OH-MDZ and 4OH-MDZ respectively. Deuterated (D_4) 1OH-MDZ, the internal standard for both analytes, was monitored at the transition m/z 346.1 to 203.1 with a collision energy of 40.

Physiologically-Based Pharmacokinetic Modeling Predictions of Drug-Drug Interactions. Dynamic PBPK modeling was used to predict the DDI of clarithromycin or erythromycin as precipitants towards MDZ as the object, utilizing the in vitro generated TDI parameters for the inhibitors in the absence and presence of varying concentrations of the PGS allosteric modulator. The SimcypTM version 21 release 1 (Certara; Princeton, NJ, USA) software was used to predict the time course of object and precipitant concentrations in plasma. The default model for MDZ (Sim-Midazolam) in SimcypTM was used as the object drug for all simulations. The SimcypTM compound files for clarithromycin (SV-Clarithromycin) and erythromycin (SV-Erythromycin) were used with minimal alterations as described below.

Clearance of clarithromycin and erythromycin in the model is predominantly metabolic with the greatest percentage of clearance attributed to CYP3A4 (fraction of systemic clearance 86% and 82% respectively). As the time-dependent inhibition of CYP3A4 by these inhibitors occurs over repeat dosing, this autoinhibition

reduces their clearance when comparing a single dose pharmacokinetics (PK) to steady state PK. The default models were optimized to capture this non-linearity through the TDI kinetic parameters and metabolic clearance pathways including CYP3A4. In order to incorporate alternate CYP3A4 TDI kinetic values determined in vitro, a non-mechanistic clearance approach was taken. Briefly, the enzyme kinetic and additional metabolic clearance pathways in the model were replaced with a total in vivo intravenous (IV) clearance. A sensitivity analysis was conducted on the in vivo IV clearance parameter to match the exposure [maximum concentration (C_{max}) and area under the concentration time curve for the dosing interval ($AUC_{0-\tau}$)] at steady state compared to the default model. An in vivo IV clearance of 14 L/h for clarithromycin and 25 L/h for erythromycin resulted in matched PK at steady state for the two precipitants and provided matched precipitant exposure (Supplemental Figure S1A,B; Table S2). The final compound file parameters for MDZ, clarithromycin and erythromycin are listed in Supplemental Table S1.

Using the new models, DDI simulations were performed for the precipitants with varying TDI kinetic parameters only. The TDI kinetic parameters reflect the in vitro experimental K_I and k_{inact} observed in the absence or presence of varying concentrations of PGS (Table 3). In vitro K_I values were corrected for the fraction unbound in microsomes ($f_{u,mic}$) of the inhibitor at the assay concentration of 0.5 mg/mL. As the unbound corrected values from Table 3 were entered directly into the model, an $f_{u,mic}$ of 1 was used as no further correction was necessary. All simulations were conducted using the healthy volunteer population (Sim-Healthy Volunteers), the number of subjects, age range and male to female ratios were modified to match the respective clinical study designs (Supplemental Table S3).

The predicted AUC ratio in the presence over the absence of precipitant (AUCR) for each simulation was plotted against the PGS concentration. Using GraphPad Prism version 10.1 (GraphPad Software, San Diego, CA, USA) a linear regression model was used to establish the relationship between PGS concentration and AUCR. This relationship was then used to extrapolate the concentration of PGS that matched the reported clinical DDI AUCR.

Data Analysis. Time-dependent inhibition parameters for K_I and k_{inact} were determined using the replot method as previously described (Silverman, 1995; Grimm et al., 2009) in GraphPad Prism version 10.1 (GraphPad Software, San Diego, CA). Values represent the mean of duplicates with an acceptance criterion of a coefficient of variance (CV) less than 20%. Inactivation efficiency, a second order rate constant relating the concentration of reactant (inhibitor potency) and rate of the reaction (inactivation rate) was calculated by taking the ratio of k_{inact} over K_I .

Results

Time-Dependent Inhibition. Graphs of the TDI replot of slope of the observed loss (k_{obs}) versus inhibitor concentration in the absence and presence of 100 μM PGS using the formation of 1OH-MDZ and 4OH-MDZ as a biomarker of CYP3A4 activity for the set of nine macrolides are presented in Figure 1 and Figure S2, respectively. The calculated TDI parameter values in the absence and presence of 100 μM PGS determined using either 1OH-MDZ or 4OH-MDZ formation as the marker of CYP3A4 activity are presented in Table 1 with K_I values corrected for the microsomal unbound fraction in the assay. Total K_I values and $f_{\text{u,mic}}$ for each compound are listed in Supplemental Table S4.

Under control conditions, clarithromycin, erythromycin, TAO, and fidaxomicin were all observed to present a TDI of CYP3A4. In the case of spiramycin, tilmicosin, and tylosin, while loss of CYP3A4 activity was observed in the control condition, the loss of enzyme activity did not exceed more than ~24% at the highest concentration tested after 60 min of incubation for all three perpetrators (data not shown). While the loss of activity exceeded the solvent control, the rates of inactivation were low and did not exceed an observed rate of loss greater than 0.153 h^{-1} (or 0.00256 min^{-1} ; observed for spiramycin).

Presence of 100 μM PGS in the assay eliminated the TDI of CYP3A4 for azithromycin, spiramycin, tilmicosin, and tylosin. Erythromycin, clarithromycin, fidaxomicin and TAO were still observed to cause TDI of CYP3A4; however, the extent of the inhibition parameters was altered. The TDI parameters observed for erythromycin, clarithromycin, and TAO trended similarly with an increase in K_I (decreased potency) and decrease in k_{inact} (reduction in inactivation rate), ranging from 1.2-fold to 8.7-fold, in the presence of PGS (Table 1). These combined changes resulted in a > 90% decrease in the inactivation efficiency potential for TAO, erythromycin, and clarithromycin (Table 2, Supplemental Table S5). However, in the case of fidaxomicin, the shift was less pronounced with a reduction of ~10% in the inactivation efficiency.

For roxithromycin, no substantial TDI signal was observed in HLM under control conditions or in the presence of 100 μM PGS. This was in contrast to the observed MIC formation in rCYP matrix (MIC Formation results;

Figure 3). A TDI kinetic assay was run for roxithromycin in rCYP enzymes confirming the inactivation of the rCYP3A4 (data not shown). Addition of 100 μ M PGS eliminated the inactivation observed under control conditions, confirming the effect of PGS in the rCYP matrix in alignment with the observed results in the MIC formation.

To determine the concentration of PGS needed *in vitro* to recapitulate the *in vivo* response of the CYP3A4 enzyme in the presence of a MBI, varying concentrations of PGS were added to the TDI assay primary incubation for clarithromycin and erythromycin. Graphs of the TDI replot are presented in Figure 2. The corresponding TDI kinetic parameters are listed in Table 3 (values for 4OH-MDZ are listed in the Supplemental Table S6). Changes in both K_I and k_{inact} were observed for the inhibitors. Erythromycin was observed to have increasing K_I (decreased potency) and decreasing k_{inact} (lower inactivation rate) in a concentration dependent manner with increasing concentrations of PGS present. The same trend of increasing K_I (decreased potency) was observed for clarithromycin; however, k_{inact} was found to increase in the presence of rising concentrations of PGS except for the 100 μ M PGS concentration, where the k_{inact} decreased.

The combination of these changes for erythromycin and clarithromycin led to decreasing inactivation efficiencies in a concentration dependent manner with PGS. It should be noted that for erythromycin, at the highest concentration of PGS tested (100 μ M), while time-dependent loss of CYP3A4 activity could still be observed at the high concentrations of inhibitor tested in the assay, the TDI did not appear to reach saturation, resulting in a linear relationship rather than an exponential relationship. Regardless, the linear slope, representing the rate of inactivation efficiency, aligned with the trend of decreasing inhibition potential with the presence of PGS.

MIC Formation. In the absence of progesterone, the perpetrators clarithromycin, erythromycin, azithromycin, spiramycin, roxithromycin, and TAO were observed to form a MIC with CYP3A4 at the 455 nm (Figure 3). When 100 μ M PGS was present in the incubation, no distinct peak at 455 nm could be observed for clarithromycin, azithromycin, spiramycin, or roxithromycin. For erythromycin and TAO, the amount of MIC

formed was reduced (Supplemental Figure S3). In the case of erythromycin, while a peak absorbance was still observed at ~455 nm in the presence of PGS, the shape of the curve was appreciably flattened. For TAO, while a distinct MIC peak was maintained in the presence of PGS, the extent of the MIC formed was reduced. No MIC formation was observed for fidaxomicin, tilmicosin, or tylosin under control conditions or in the presence of PGS.

PBPK DDI Modeling. Predictions of the interactions between clarithromycin or erythromycin towards MDZ were conducted using clinical study designs reported in the literature. Each study design was repeated with the different TDI kinetic parameters determined in the presence of varying concentrations of PGS reported in Table 2. The predicted AUCR for a single study design was then plotted against the PGS concentrations used. A linear regression analysis was performed by which the extrapolated concentration of PGS was determined that would result in the clinically observed AUCR. All r-squared values for the Pearson correlation were ≥ 0.85 for erythromycin and ≥ 0.95 for clarithromycin. A representative example is presented in Figure 4 (all studies are shown in Supplemental Material Figure S4). The interpolated concentrations of PGS predicted for each set of clinical studies for erythromycin and clarithromycin are listed in Table 4, with an average concentration of 45.5 μM of PGS across both inhibitors predicted to represent the concentration of PGS needed in the in vitro assay that would result in TDI kinetic parameters that would capture the in vivo TDI.

Discussion (1588 words)

In the present study, nine macrolide molecules were found to cause time-dependent inhibition of CYP3A4 in HLM under control conditions aligning with previous observations (Polasek and Miners, 2006; Eng et al., 2020; Yamada et al., 2020). While the mechanism of TDI of the macrolide class of drugs has been attributed to the formation of a metabolic-intermediate complex (MIC) (Pershing and Franklin, 1982), only six of the nine molecules were observed to form the MIC complex (Figure 3). For tilmicosin, tylosin, and fidaxomicin, molecules that did not form a MIC in this study, we are not aware of reports to the contrary in human matrices (either microsomal or recombinant). Investigations using rat, rabbit, goat, and cattle microsomes have reported the lack of MIC formation for tilmicosin (Zweers-Zeilmaker et al., 1999; Carletti et al., 2003). Interestingly, tylosin has been observed to form an MIC in these animal matrices (Zweers-Zeilmaker et al., 1999; Carletti et al., 2003). Fidaxomicin lacks an amine group that leads to the hallmark formation of a reactive nitroso amine intermediate that forms the complex with the heme iron in the CYP enzymes and may therefore not elicit inactivation through this mechanism (Taxak et al., 2012). Regardless of MIC formation, for tilmicosin and tylosin, these compounds elicit weak to negligible loss of CYP3A4 activity at high concentrations in in vitro matrices (current work; Zweers-Zeilmaker et al. (1999); Carletti et al. (2003)) and have not been found to impact the PK of CYP3A4 substrates in vivo (Anadón and Reeve-johnson, 1999), suggesting a lack of translation of the in vitro TDI signal for these two molecules.

Previous work demonstrated that the presence of allosteric modulators in in vitro assays, such as the endogenous androgen progesterone or chemical substrate carbamazepine, can alter the metabolic function of CYP3A4 (Nakamura et al., 2002; Nakamura et al., 2003; Cameron et al., 2005; Roberts et al., 2011; Denisov et al., 2022; Rougée et al., 2023). For PGS, collective evidence suggests that these changes are a result of PGS interaction with the characterized allosteric binding site of CYP3A4 and not direct competition within the enzyme's active site (Williams et al., 2004; Denisov et al., 2007; Polic and Auclair, 2017; Denisov et al., 2021; Denisov et al., 2022; Rougée et al., 2023). Interaction of PGS with this allosteric site modified the TDI kinetics of CYP3A4 mechanism-based inhibitors (MBI), when the mechanism involves interaction with the heme

moiety (MIC and heme destruction) (Rougée et al., 2023). The current study confirms these previous findings for the MIC forming inhibitors, clarithromycin and TAO, and is consistent with the allosteric binding of PGS resulting in a conformational change of CYP3A4 (Denisov et al., 2015a; Denisov et al., 2015b; Denisov et al., 2019), that leads to the reduced capability of forming a stable inactivation complex for MIC forming MBIs.

Investigation into the basis of substrate dependent differences in inhibition of CYP3A4 by Wei et al. (2024) may provide further insight. Reversible inhibition constants (K_i) of the inhibitors erdafitinib and pemigatinib were found to be more potent when using rivaroxaban as the probe substrate for CYP3A4 activity compared to testosterone (TST). Molecular dynamic (MD) simulations reported that binding of the allosteric site of CYP3A4 by erdafitinib and pemigatinib reduced the flexibility of the F–F' loop, a well-established region of the enzyme involved in the regulation of the active site opening, access, and conformational binding (Ekroos and Sjögren, 2006; Fishelovitch et al., 2009; Denisov et al., 2019). Denisov et al. (2019) demonstrated experimentally and with MD simulations that PGS interaction with this phenylalanine cluster impacts the CYP3A4 metabolism of CBZ. While Wei et al. (2024) attribute the changes in inhibition to the interaction of the inhibitors with the allosteric site, resulting in restricted access of the larger rivaroxaban substrate to the active site, this may not be entirely the case. Homotropic cooperativity has been observed for TST, with the atypical kinetics of its metabolism being attributable to TST binding the allosteric CYP3A4 site first, with subsequent binding events of up to two more TST occurring in the active site (Harlow and Halpert, 1998; Denisov et al., 2007; Denisov et al., 2015b). Interaction with the allosteric binding site has been further shown through heterotropic cooperativity of TST with the prototypical CYP3A4 substrate, midazolam (MDZ), whereby the binding of TST to the allosteric site produces conformational changes in the enzyme active site that orient the MDZ substrate towards the heme and recapitulate the homotropic metabolite production of MDZ only observed at higher concentrations of the substrate (Fu, Zhang and Zheng, 2022; Rougée et al., 2023). The Michaelis-Menten constant (K_m) or affinity of TST for the CYP3A4 active site ranges from 72 to 97 μM (Yamazaki and Shimada, 1997), indicating that it is not a particular strong substrate for CYP3A4 (albeit a selective one). While TST could exert some competition for the initial binding to the active site at high concentrations, at lower

concentrations of TST (50 μM in the case of the work by Wei et al. (2024)), combined with the lower K_m of MDZ ($\sim 4 \mu\text{M}$) and more potent K_i values for erdafitinib and pemigatinib reported at 10.2 and 3.3 μM respectively, it is more likely that the difference in substrate-dependent metabolism or inhibition is a result of allosteric modulation by TST binding to the allosteric site.

PGS also exhibits a low affinity for the CYP3A4 active site with K_m estimates between 80 to 96 μM (Yamazaki and Shimada, 1997) and therefore its impact on MBI is likely through the allosteric binding site. The hypothesis that PGS only competes directly with the MBI for the active site appears unlikely because higher concentrations of inhibitor would be expected to outcompete the PGS and eventually lead to inactivation. This was not observed with inhibitors whose range tested was up to 2.5-fold higher than the PGS concentration in the assay yet yielded no inactivation up to 1 hour of pre-incubation. Combined with the simultaneous changes in both K_I and k_{inact} inhibition kinetic parameters for well-established MBI (clarithromycin, TAO, erythromycin), and lack of effect of PGS on the TDI by fidaxomicin, the impact of PGS appears to be predominantly at the allosteric site of CYP3A4.

Translation of the in vitro finding observed for azithromycin, the disappearance of the TDI signal in the presence of PGS, aligns with the lack of observed clinical interaction (Yeates et al., 1997). In the case of fidaxomicin, no clinical DDI has been reported either, yet the TDI signal in vitro was maintained in the presence of PGS. Allosteric modulation has been shown to be dependent on the enzyme/substrate and enzyme/substrate/inhibitor combinations. Fidaxomicin findings indicates that the impact of PGS with the allosteric site of CYP3A4 may not interfere with the mechanism of inactivation of fidaxomicin which is not through MIC. Fidaxomicin serves as an example highlighting the importance of interpreting the TDI risk in context of the bigger picture. In the clinical interaction study conducted, fidaxomicin was administered at 200 mg twice daily for 4 days (NDA-201699, 2010). After multiple dosing, fidaxomicin reached a maximum plasma concentration of $\sim 4.9 \text{ nM}$ (NDA-201699, 2010), which is well below the measured K_I in vitro, indicating that the TDI in vitro is a true positive, but that the interaction is unlikely to occur in vivo as the exposure does not reach levels capable of eliciting a measurable inactivation.

The current study demonstrates the potential predictive improvement of the addition of the allosteric modulator PGS to the artifactual HLM matrix by eliminating false positives while retaining true MBI signal and potentially improving TDI kinetic values that may predict the extent of DDI using in vitro data a priori. Dynamic simulations for the well-established clinical TDIs, erythromycin and clarithromycin, suggest that the presence of ~45 μM PGS results in in vitro TDI parameters in HLM that capture the range of observed clinical DDIs for these inhibitors. However, this concentration is much higher than reported circulating concentrations of PGS that vary with age, gender and reproductive cycle peaking between ~31 to 110 nM (Elmlinger, Kühnel and Ranke, 2002; Taraborrelli, 2015). Incorporation of a mechanistic modeling approach including some of the complexities associated with atypical inactivation kinetics may reduce the concentration of PGS needed in vitro and warrants further consideration. However, the addition of PGS in the artificial HLM matrix is not meant to replicate circulating PGS levels in vivo, but to mimic the holistic interaction of all endogenous substrates and allosteric binders that may interact with the CYP3A4 allosteric site that would influence the inactivation in vivo. Other endogenous steroids including testosterone (6.34 nM), 17α -hydroxyprogesterone (1.84 nM), cortisol (264 nM), androstenedione (3.21 nM), pregnenolone (5.06 nM), aldosterone (0.14 nM), dehydroepiandrosterone (10.3 nM), and dehydroepiandrosterone-sulfate (4163 nM) have all demonstrated in vitro cooperativity towards CYP3A4 and may contribute to the allosteric modulation in vivo [values represent median plasma concentrations reported for combined adult males and females (Eisenhofer et al., 2017)]. It is worth noting that the levels reported for steroids are systemic circulating levels. As the liver is a major site of steroidogenesis and metabolism, it is possible that the concentrations of some steroids may be greater at the level of the tissue during intracrinology (the process by which a tissue uses blood precursors to produce steroids) and in the process of their elimination from circulation (Miller and Auchus, 2011; Schiffer et al., 2019). Further investigation using the identified representative PGS concentration across a variety of in vitro, identified CYP3A4 TDI compounds is needed to understand the translative power of adding the allosteric modulator PGS to in vitro HLM TDI assays.

Acknowledgements

None

Data Availability Statement

The authors declare that all the data supporting the findings of this study are available within the paper and its Supplemental Data.

Authorship Contributions

Participated in research design: Rougée, Hall

Conducted experiments: Rougée, Hegde, Shin, Abraham, Bell

Contributed new reagents or analytical tools: Abraham, Bell

Performed data analysis: Rougée, Hegde, Shin, Hall

Wrote or contributed to the writing of the manuscript: Rougée, Hegde, Hall

References

- Anadón A and Reeve-johnson L (1999) Macrolide antibiotics, drug interactions and microsomal enzymes: implications for veterinary medicine. *Res Vet Sci* **66**:197-203.
- Cameron MD, Wen B, Allen KE, Roberts AG, Schuman JT, Campbell AP, Kunze KL, and Nelson SD (2005) Cooperative binding of midazolam with testosterone and alpha-naphthoflavone within the CYP3A4 active site: a NMR T1 paramagnetic relaxation study. *Biochemistry* **44**:14143-14151.
- Carletti M, Gusson F, Zaghini A, Dacasto M, Marvasi L, and Nebbia C (2003) In vitro formation of metabolic-intermediate cytochrome P450 complexes in rabbit liver microsomes by tiamulin and various macrolides. *Vet Res* **34**:405-411.
- Denisov IG, Baas BJ, Grinkova YV, and Sligar SG (2007) Cooperativity in cytochrome P450 3A4: linkages in substrate binding, spin state, uncoupling, and product formation. *J Biol Chem* **282**:7066-7076.
- Denisov IG, Grinkova YV, Baylon JL, Tajkhorshid E, and Sligar SG (2015a) Mechanism of drug-drug interactions mediated by human cytochrome P450 CYP3A4 monomer. *Biochemistry* **54**:2227-2239.
- Denisov IG, Grinkova YV, Camp T, McLean MA, and Sligar SG (2021) Midazolam as a Probe for Drug-Drug Interactions Mediated by CYP3A4: Homotropic Allosteric Mechanism of Site-Specific Hydroxylation. *Biochemistry* **60**:1670-1681.
- Denisov IG, Grinkova YV, McLean MA, Camp T, and Sligar SG (2022) Midazolam as a Probe for Heterotropic Drug-Drug Interactions Mediated by CYP3A4. *Biomolecules* **12**:853.
- Denisov IG, Grinkova YV, Nandigrami P, Shekhar M, Tajkhorshid E, and Sligar SG (2019) Allosteric Interactions in Human Cytochrome P450 CYP3A4: The Role of Phenylalanine 213. *Biochemistry* **58**:1411-1422.
- Denisov IG, Mak PJ, Grinkova YV, Bastien D, Berube G, Sligar SG, and Kincaid JR (2015b) The use of isomeric testosterone dimers to explore allosteric effects in substrate binding to cytochrome P450 CYP3A4. *J Inorg Biochem*.
- Eisenhofer G, Peitzsch M, Kaden D, Langton K, Pamporaki C, Masjkur J, Tsatsaronis G, Mangelis A, Williams TA, Reincke M, Lenders JWM, and Bornstein SR (2017) Reference intervals for plasma concentrations of adrenal steroids measured by LC-MS/MS: Impact of gender, age, oral contraceptives, body mass index and blood pressure status. *Clin Chim Acta* **470**:115-124.
- Ekroos M and Sjögren T (2006) Structural basis for ligand promiscuity in cytochrome P450 3A4. *Proceedings of the National Academy of Sciences* **103**:13682.
- Elmlinger MW, Kühnel W, and Ranke MB (2002) Reference ranges for serum concentrations of lutropin (LH), follitropin (FSH), estradiol (E2), prolactin, progesterone, sex hormone-binding globulin (SHBG), dehydroepiandrosterone sulfate (DHEAS), cortisol and ferritin in neonates, children and young adults. *Clin Chem Lab Med* **40**:1151-1160.
- Eng H, Tseng E, Cerny MA, Goosen TC, and Obach RS (2020) Cytochrome P450 3A Time-Dependent Inhibition Assays Are Too Sensitive for Identification of Drugs Causing Clinically Significant Drug-Drug Interactions: A Comparison of Human Liver Microsomes and Hepatocytes and Definition of Boundaries for Inactivation Rate Constants. *Drug Metab Dispos* **49**:442-450.
- Filppula AM, Parvizi R, Mateus A, Baranczewski P, and Artursson P (2019) Improved predictions of time-dependent drug-drug interactions by determination of cytosolic drug concentrations. *Sci Rep* **9**:5850.
- Fishelovitch D, Shaik S, Wolfson HJ, and Nussinov R (2009) Theoretical Characterization of Substrate Access/Exit Channels in the Human Cytochrome P450 3A4 Enzyme: Involvement of Phenylalanine Residues in the Gating Mechanism. *The Journal of Physical Chemistry B* **113**:13018-13025.
- Fohner AE, Sparreboom A, Altman RB, and Klein TE (2017) PharmGKB summary: Macrolide antibiotic pathway, pharmacokinetics/pharmacodynamics. *Pharmacogenet Genomics* **27**:164-167.
- Fu T, Zhang H, and Zheng Q (2022) Molecular Insights into the Heterotropic Allosteric Mechanism in Cytochrome P450 3A4-Mediated Midazolam Metabolism. *J Chem Inf Model* **62**:5762-5770.

- Gorski JC, Jones DR, Haehner-Daniels BD, Hamman MA, O'Mara Jr EM, and Hall SD (1998) The contribution of intestinal and hepatic CYP3A to the interaction between midazolam and clarithromycin. *Clinical Pharmacology & Therapeutics* **64**:133-143.
- Gurley BJ, Swain A, Hubbard MA, Hartsfield F, Thaden J, Williams DK, Gentry WB, and Tong Y (2008) Supplementation With Goldenseal (*Hydrastis canadensis*), but not Kava Kava (*Piper methysticum*), Inhibits Human CYP3A Activity In Vivo. *Clinical Pharmacology & Therapeutics* **83**:61-69.
- Harlow GR and Halpert JR (1998) Analysis of human cytochrome P450 3A4 cooperativity: construction and characterization of a site-directed mutant that displays hyperbolic steroid hydroxylation kinetics. *Proc Natl Acad Sci U S A* **95**:6636-6641.
- Korzekwa K, Tweedie D, Argikar UA, Whitcher-Johnstone A, Bell L, Bickford S, and Nagar S (2014) A numerical method for analysis of in vitro time-dependent inhibition data. Part 2. Application to experimental data. *Drug Metab Dispos* **42**:1587-1595.
- Lee S, Lee Y, Kim AH, Yoon S, Lee J, Ji SC, Yoon SH, Lee S, Yu K-S, Jang I-J, and Cho J-Y (2021) Urinary metabolic markers reflect on hepatic, not intestinal, CYP3A activity in healthy subjects. *Drug Metabolism and Pharmacokinetics* **36**:100374.
- Miller WL and Auchus RJ (2011) The molecular biology, biochemistry, and physiology of human steroidogenesis and its disorders. *Endocr Rev* **32**:81-151.
- Nagar S, Jones JP, and Korzekwa K (2014) A numerical method for analysis of in vitro time-dependent inhibition data. Part 1. Theoretical considerations. *Drug Metab Dispos* **42**:1575-1586.
- Nakamura H, Nakasa H, Ishii I, Ariyoshi N, Igarashi T, Ohmori S, and Kitada M (2002) Effects of endogenous steroids on CYP3A4-mediated drug metabolism by human liver microsomes. *Drug Metab Dispos* **30**:534-540.
- Nakamura H, Torimoto N, Ishii I, Ariyoshi N, Nakasa H, Ohmori S, and Kitada M (2003) CYP3A4 and CYP3A7-mediated carbamazepine 10,11-epoxidation are activated by differential endogenous steroids. *Drug Metab Dispos* **31**:432-438.
- NDA-201699 (2010) Optimer Pharmaceuticals, Inc. (2010) Center for Drug Evaluation and Research: Application Number 201699. Clinical Pharmacology and Biopharmaceutics Review . https://www.accessdata.fda.gov/drugsatfda_docs/nda/2011/201699Orig1s000ClinPharmR.pdf.
- Obach RS, Walsky RL, and Venkatakrisnan K (2007) Mechanism-based inactivation of human cytochrome p450 enzymes and the prediction of drug-drug interactions. *Drug Metab Dispos* **35**:246-255.
- Obach RS, Walsky RL, Venkatakrisnan K, Gaman EA, Houston JB, and Tremaine LM (2006) The utility of in vitro cytochrome P450 inhibition data in the prediction of drug-drug interactions. *J Pharmacol Exp Ther* **316**:336-348.
- Okudaira T, Kotegawa T, Imai H, Tsutsumi K, Nakano S, and Ohashi K (2007) Effect of the Treatment Period With Erythromycin on Cytochrome P450 3A Activity in Humans. *The Journal of Clinical Pharmacology* **47**:871-876.
- Olkkola KT, Aranko K, Luurila H, Hiller A, Saarnivaara L, Himberg J-J, and Neuvonen PJ (1993) A potentially hazardous interaction between erythromycin and midazolam. *Clinical Pharmacology & Therapeutics* **53**:298-305.
- Pershing LK and Franklin MR (1982) Cytochrome P-450 metabolic-intermediate complex formation and induction by macrolide antibiotics; a new class of agents. *Xenobiotica* **12**:687-699.
- Polasek TM and Miners JO (2006) Quantitative prediction of macrolide drug-drug interaction potential from in vitro studies using testosterone as the human cytochrome P4503A substrate. *Eur J Clin Pharmacol* **62**:203-208.
- Polic V and Auclair K (2017) Allosteric Activation of Cytochrome P450 3A4 via Progesterone Bioconjugation. *Bioconjug Chem* **28**:885-889.
- Prueksaritanont T, Tatosian DA, Chu X, Railkar R, Evers R, Chavez-Eng C, Lutz R, Zeng W, Yabut J, Chan GH, Cai X, Latham AH, Hehman J, Stypinski D, Brejda J, Zhou C, Thornton B, Bateman KP, Fraser I, and Stoch SA (2017) Validation of a microdose probe drug cocktail for clinical drug interaction assessments for drug transporters and CYP3A. *Clinical Pharmacology & Therapeutics* **101**:519-530.

- Quinney SK, Haehner BD, Rhoades MB, Lin Z, Gorski JC, and Hall SD (2008) Interaction between midazolam and clarithromycin in the elderly. *British Journal of Clinical Pharmacology* **65**:98-109.
- Roberts AG, Yang J, Halpert JR, Nelson SD, Thummel KT, and Atkins WM (2011) The structural basis for homotropic and heterotropic cooperativity of midazolam metabolism by human cytochrome P450 3A4. *Biochemistry* **50**:10804-10818.
- Rostami-Hodjegan A and Tucker G (2004) 'In silico' simulations to assess the 'in vivo' consequences of 'in vitro' metabolic drug-drug interactions. *Drug Discov Today Technol* **1**:441-448.
- Rougée LRA, Bedwell DW, Hansen K, Abraham TL, and Hall SD (2023) Impact of Heterotropic Allosteric Modulation on the Time-Dependent Inhibition of Cytochrome P450 3A4. *Drug Metab Dispos* **51**:1372-1380.
- Schiffer L, Barnard L, Baranowski ES, Gilligan LC, Taylor AE, Arlt W, Shackleton CHL, and Storbeck KH (2019) Human steroid biosynthesis, metabolism and excretion are differentially reflected by serum and urine steroid metabolomes: A comprehensive review. *J Steroid Biochem Mol Biol* **194**:105439.
- Taraborrelli S (2015) Physiology, production and action of progesterone. *Acta Obstet Gynecol Scand* **94 Suppl 161**:8-16.
- Taxak N, Desai PV, Patel B, Mohutsky M, Klimkowski VJ, Gombar V, and Bharatam PV (2012) Metabolic-intermediate complex formation with cytochrome P450: theoretical studies in elucidating the reaction pathway for the generation of reactive nitroso intermediate. *J Comput Chem* **33**:1740-1747.
- Tseng E, Eng H, Lin J, Cerny MA, Tess DA, Goosen TC, and Obach RS (2021) Static and Dynamic Projections of Drug-Drug Interactions Caused by Cytochrome P450 3A Time-Dependent Inhibitors Measured in Human Liver Microsomes and Hepatocytes. *Drug Metab Dispos* **49**:947-960.
- Vieira MLT, Kirby B, Ragueneau-Majlessi I, Galetin A, Chien JYL, Einolf HJ, Fahmi OA, Fischer V, Fretland A, Grime K, Hall SD, Higgs R, Plowchalk D, Riley R, Seibert E, Skordos K, Snoeys J, Venkatakrishnan K, Waterhouse T, Obach RS, Berglund EG, Zhang L, Zhao P, Reynolds KS, and Huang S-M (2014) Evaluation of Various Static In Vitro–In Vivo Extrapolation Models for Risk Assessment of the CYP3A Inhibition Potential of an Investigational Drug. *Clin Pharmacol Ther* **95**:189-198.
- von Rosensteil NA and Adam D (1995) Macrolide antibacterials. Drug interactions of clinical significance. *Drug Saf* **13**:105-122.
- Wei W, Tang LWT, Verma RK, Fan H, and Chan ECY (2024) Probe Substrate Dependencies in CYP3A4 Allosteric Inhibition: A Novel Molecular Mechanism Involving F-F' Loop Perturbations. *J Chem Inf Model*.
- Westphal JF (2000) Macrolide - induced clinically relevant drug interactions with cytochrome P-450A (CYP) 3A4: an update focused on clarithromycin, azithromycin and dirithromycin. *Br J Clin Pharmacol* **50**:285-295.
- Williams PA, Cosme J, Vinkovic DM, Ward A, Angove HC, Day PJ, Vonnrhein C, Tickle IJ, and Jhoti H (2004) Crystal structures of human cytochrome P450 3A4 bound to metyrapone and progesterone. *Science* **305**:683-686.
- Yadav J, Korzekwa K, and Nagar S (2018) Improved Predictions of Drug-Drug Interactions Mediated by Time-Dependent Inhibition of CYP3A. *Mol Pharm* **15**:1979-1995.
- Yamada M, Inoue SI, Sugiyama D, Nishiya Y, Ishizuka T, Watanabe A, Watanabe K, Yamashita S, and Watanabe N (2020) Critical Impact of Drug-Drug Interactions via Intestinal CYP3A in the Risk Assessment of Weak Perpetrators Using Physiologically Based Pharmacokinetic Models. *Drug Metab Dispos* **48**:288-296.
- Yamazaki H and Shimada T (1997) Progesterone and Testosterone Hydroxylation by Cytochromes P450 2C19, 2C9, and 3A4 in Human Liver Microsomes. *Arch Biochem Biophys* **346**:161-169.
- Yeates RA, Laufen H, Zimmermann T, and Schumacher T (1997) Pharmacokinetic and pharmacodynamic interaction study between midazolam and the macrolide antibiotics, erythromycin, clarithromycin, and the azalide azithromycin. *Int J Clin Pharmacol Ther* **35**:577-579.

- Zimmermann T, Yeates RA, Laufen H, Scharpf F, Leitold M, and Wildfeuer A (1996) Influence of the antibiotics erythromycin and azithromycin on the pharmacokinetics and pharmacodynamics of midazolam. *Arzneimittelforschung* **46**:213-217.
- Zweers-Zeilmaker WM, Van Miert AS, Horbach GJ, and Witkamp RF (1999) In vitro complex formation and inhibition of hepatic cytochrome P450 activity by different macrolides and tiamulin in goats and cattle. *Res Vet Sci* **66**:51-55.

Footnotes

This work received no external funding.

No author has an actual or perceived conflict of interest with the contents of this article.

Figure Legends

Figure 1. Replot analysis of mechanism-based inhibitors in the absence and presence of 100 μ M PGS using 1OH-MDZ formation to quantify CYP3A4 activity. (A) Azithromycin; (B) Erythromycin; (C) Clarithromycin; (D) Spiramycin; (E) Fidaxomicin; (F) Troleandomycin; (G) Tilmicosin; (H) Tylosin. Closed circles with solid line represent assays in the absence of PGS in the primary incubation and closed squares with a dashed line represent assays in the presence of 100 μ M PGS in the primary incubation.

Figure 2: Time-dependent inhibition of CYP3A4 by clarithromycin or erythromycin with varying PGS concentrations using 1-OH MDZ or 4-OH MDZ formation to quantify CYP3A4 activity. (A) Clarithromycin inhibition of CYP3A4 measured using 1OH-MDZ; (B) Erythromycin inhibition of CYP3A4 measured using 1OH-MDZ; (C) Clarithromycin inhibition of CYP3A4 measured using 4OH-MDZ; (D) Erythromycin inhibition of CYP3A4 measured using 4OH-MDZ. Control (\bullet), 1 μ M progesterone (\blacksquare), 10 μ M progesterone (\diamond), 20 μ M progesterone (\odot), 40 μ M progesterone (\circ), 60 μ M progesterone (\square), 80 μ M progesterone (Δ), 100 μ M progesterone (\times).

Figure 3: Metabolic-intermediate complex formation of mechanism-based inhibitors in the absence or presence of 100 μ M PGS. (A) Clarithromycin; (B) Erythromycin; (C) Azithromycin; (D) Spiramycin; (E) Roxithromycin; (F) Troleandomycin. The solid black line represents inhibitor alone, the dashed line represents the inhibitor in the presence of 100 μ M PGS.

Figure 4: Predicted interactions of MDZ with clarithromycin or erythromycin using in vitro time-dependent kinetic parameters established in varying concentrations of PGS. (A) Predicted interactions of MDZ with clarithromycin; (B) Predicted interactions of MDZ with erythromycin. Results presented for study 1 listed in Table 1 for each inhibitor. Solid line represents the mean value for the linear regression while the dotted lines around it represent the 95% confidence intervals. The horizontal dashed line represents the clinically observed AUC ratio, with the vertical dashed line representing the interpolated concentration of progesterone.

Tables

Table 1. Time-dependent CYP3A4 inhibition kinetic parameters in the absence and presence of 100 μ M PGS using 1OH-MDZ or 4OH-MDZ formation to quantify CYP3A4 activity.

Inhibitor	1OH-MDZ				4OH-MDZ			
	Control		100 μ M PGS		Control		100 μ M PGS	
	$K_{I,u}$ (μ M)	k_{inact} (h^{-1})	$K_{I,u}$ (μ M)	k_{inact} (h^{-1})	$K_{I,u}$ (μ M)	k_{inact} (h^{-1})	$K_{I,u}$ (μ M)	k_{inact} (h^{-1})
Azithromycin	259 \pm 238	1.07 \pm 0.72	ND	ND	277 \pm 123	1.05 \pm 0.34	ND	ND
Erythromycin	12.4 \pm 2.45	2.21 \pm 0.20	1168 \pm 1117	5.92 \pm 5.50	10.6 \pm 2.40	2.11 \pm 0.20	446 \pm 306	3.26 \pm 0.20
Clarithromycin	8.41 \pm 0.73	1.95 \pm 0.90	47.7 \pm 5.61	1.02 \pm 0.60	5.52 \pm 0.30	1.24 \pm 0.02	44.6 \pm 15.9	0.55 \pm 0.11
Troleandomycin	1.89 \pm 1.72	6.18 \pm 1.05	16.5 \pm 8.17	0.91 \pm 0.32	6.55 \pm 2.25	7.69 \pm 1.46	19.1 \pm 12.6	1.11 \pm 0.55
Roxithromycin	ND	ND	ND	ND	ND	ND	ND	ND
Fidaxomicin	75.7 \pm 43.3	9.76 \pm 3.90	88.9 \pm 88.4	10.4 \pm 7.58	30.5 \pm 17.0	5.64 \pm 1.68	53.4 \pm 53.0	7.06 \pm 4.44
Spiramycin	61.7 \pm 47.0	0.17 \pm 0.01	ND	ND	29.9 \pm 19.9	0.19 \pm 0.01	ND	ND
Tilmicosin	123 \pm 128	0.24 \pm 0.12	ND	ND	321 \pm 82.7	0.32 \pm 0.06	ND	ND
Tylosin	127 \pm 10.2	0.16 \pm 0.01	ND	ND	181 \pm 80.5	0.17 \pm 0.01	ND	ND

Mean best fit values and standard error are reported.

Abbreviations: h, hour, $K_{I,u}$, unbound irreversible inhibition constant, inhibitor concentration at which half the maximal rate constant occurs; k_{inact} , first order inactivation rate constant; PGS, progesterone; μ M, micromolar; 1OH-MDZ, 1'-hydroxymidazolam; 4OH-MDZ, 4'-hydroxymidazolam; ND, not detected.

Table 2. Inactivation efficiency of time-dependent CYP3A4 inhibition in the absence and presence of 100 μ M PGS using 1OH-MDZ formation to quantify CYP3A4 activity.

Inhibitor	Inactivation Efficiency ($\text{nM}^{-1} \cdot \text{h}^{-1}$)		% Decrease from Control
	Control	100 μ M PGS	
Azithromycin	4.12	0.00	100
Erythromycin	178	5.07	97.2
Clarithromycin	232	21.4	90.8
Troleandomycin	3270	55.3	98.3
Roxithromycin	ND	ND	ND
Fidaxomicin	129	117	8.98
Spiramycin	2.75	0.00	100
Tilmicosin	1.94	0.00	100
Tylosin	1.26	0.00	100

Abbreviations: h, hour; ND, not detected; nM, nanomolar; PGS, progesterone.

Table 3. Time-dependent CYP3A4 inhibition kinetic parameters for clarithromycin and erythromycin in the absence and presence of varying concentrations of PGS using 1OH-MDZ formation to quantify CYP3A4 activity.

PGS Conc. (μM)	Erythromycin			Clarithromycin		
	$K_{I,u}$ (μM)	k_{inact} (h^{-1})	Inactivation efficiency ($\text{nM}^{-1}\cdot\text{h}^{-1}$)	$K_{I,u}$ (μM)	k_{inact} (h^{-1})	Inactivation efficiency ($\text{nM}^{-1}\cdot\text{h}^{-1}$)
Control	12.5 ± 2.45	2.21 ± 0.20	176.04	8.41 ± 0.73	1.95 ± 0.89	231
1	12.0 ± 2.11	2.06 ± 0.10	170.49	8.00 ± 1.42	1.75 ± 0.91	219
10	15.3 ± 3.02	1.89 ± 0.20	123.29	11.3 ± 2.00	1.80 ± 0.61	160
20	15.6 ± 4.94	1.58 ± 0.20	105.64	14.3 ± 2.30	1.90 ± 0.80	133
40	19.6 ± 2.45	0.91 ± 0.10	43.76	20.3 ± 3.42	2.09 ± 0.50	103
60	30.1 ± 5.67	0.89 ± 0.10	29.30	35.3 ± 4.83	2.32 ± 0.50	66.0
80	56.2 ± 23.6	0.92 ± 0.20	16.35	40.6 ± 6.79	2.52 ± 0.60	62.2
100	1168 ± 1117^a	5.92 ± 5.50^a	5.04^a	47.7 ± 5.61	1.02 ± 0.60	21.4

^a Asymptotic curve was poorly defined. Slope of the linear plot was $2.43 \text{ nM}^{-1}\cdot\text{h}^{-1}$.

Mean best fit values and standard error are reported.

Abbreviations: h, hour; $K_{I,u}$, unbound irreversible inhibition constant, inhibitor concentration at which half the maximal rate constant occurs; k_{inact} , first order inactivation rate constant; nM, nanomolar; PGS, progesterone; μM , micromolar; 1OH-MDZ, 1'-hydroxymidazolam

Table 4. Interpolated in vitro progesterone assay concentrations needed to recapitulate observed clinical inhibition for erythromycin and clarithromycin.

Inhibitor	Study No.	Progesterone Conc (μM)	Reference
<i>Erythromycin</i>	1	41.2	<u>(Olkkola et al., 1993)</u>
	2	55.4	<u>(Olkkola et al., 1993)</u>
	3	60.0	<u>(Zimmermann et al., 1996)</u>
	4	52.1	<u>(Okudaira et al., 2007)</u>
	5	42.9	<u>(Okudaira et al., 2007)</u>
<i>Clarithromycin</i>	1	54.0	<u>(Gurley et al., 2008)</u>
	2	33.0	<u>(Gorski et al., 1998)</u>
	3	43.1	<u>(Quinney et al., 2008)</u>
	4	38.2	<u>(Lee et al., 2021)</u>
	5	57.6	<u>(Prueksaritanont et al., 2017)</u>
	6	33.6	<u>(Gorski et al., 1998)</u>
	7	35.5	<u>(Quinney et al., 2008)</u>
Average (\pm SD)		45.5 \pm 9.78	

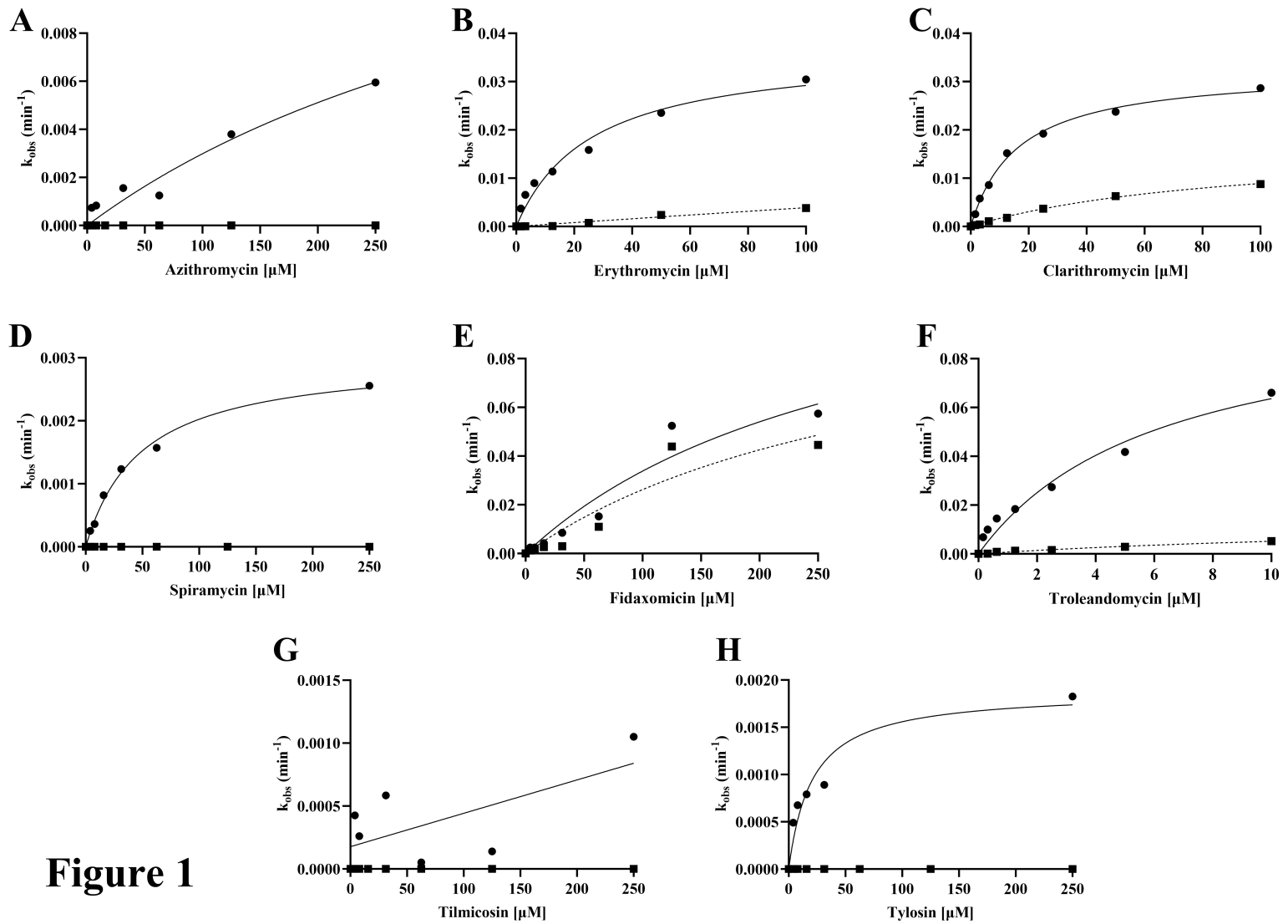


Figure 1

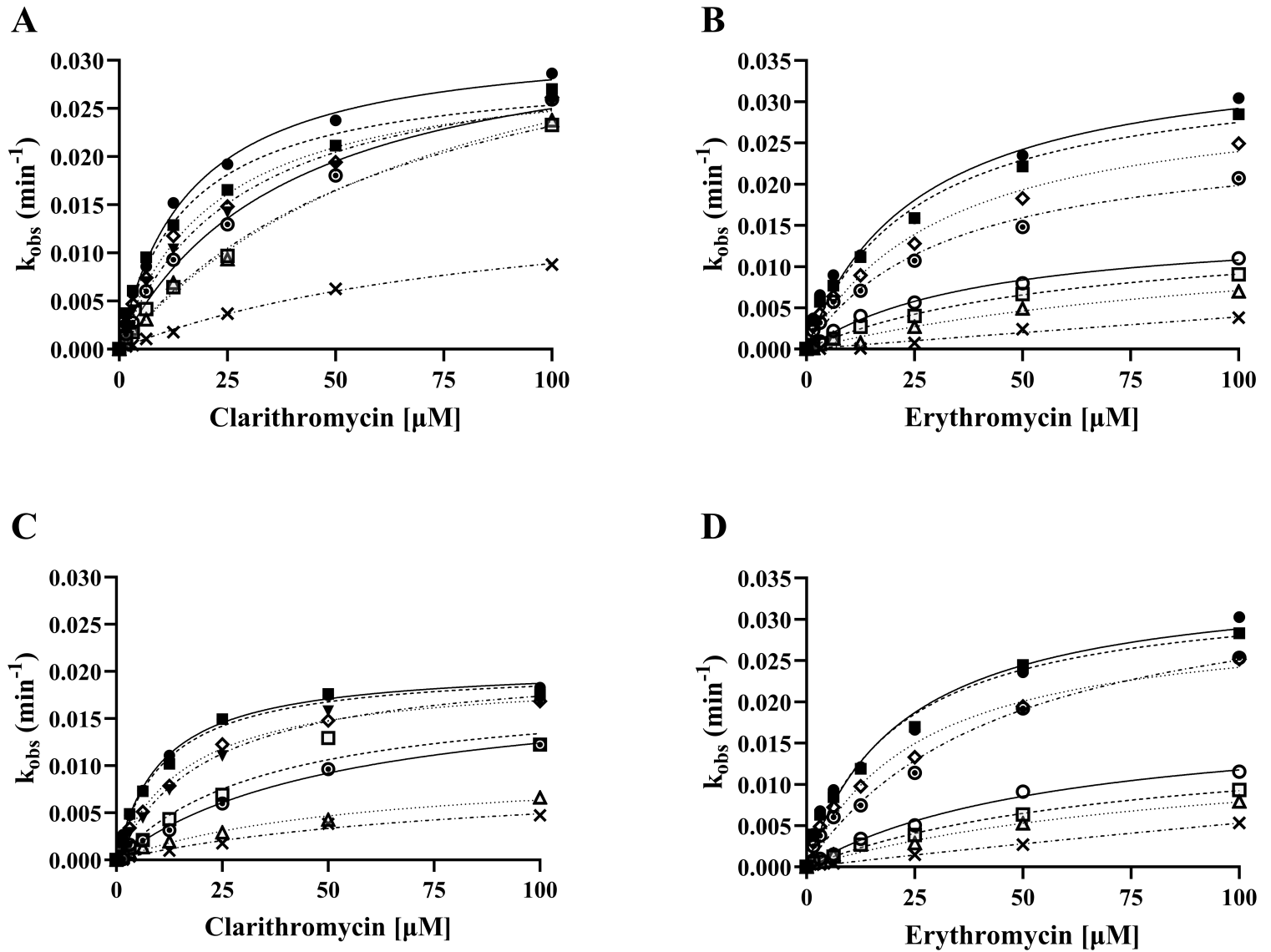


Figure 2

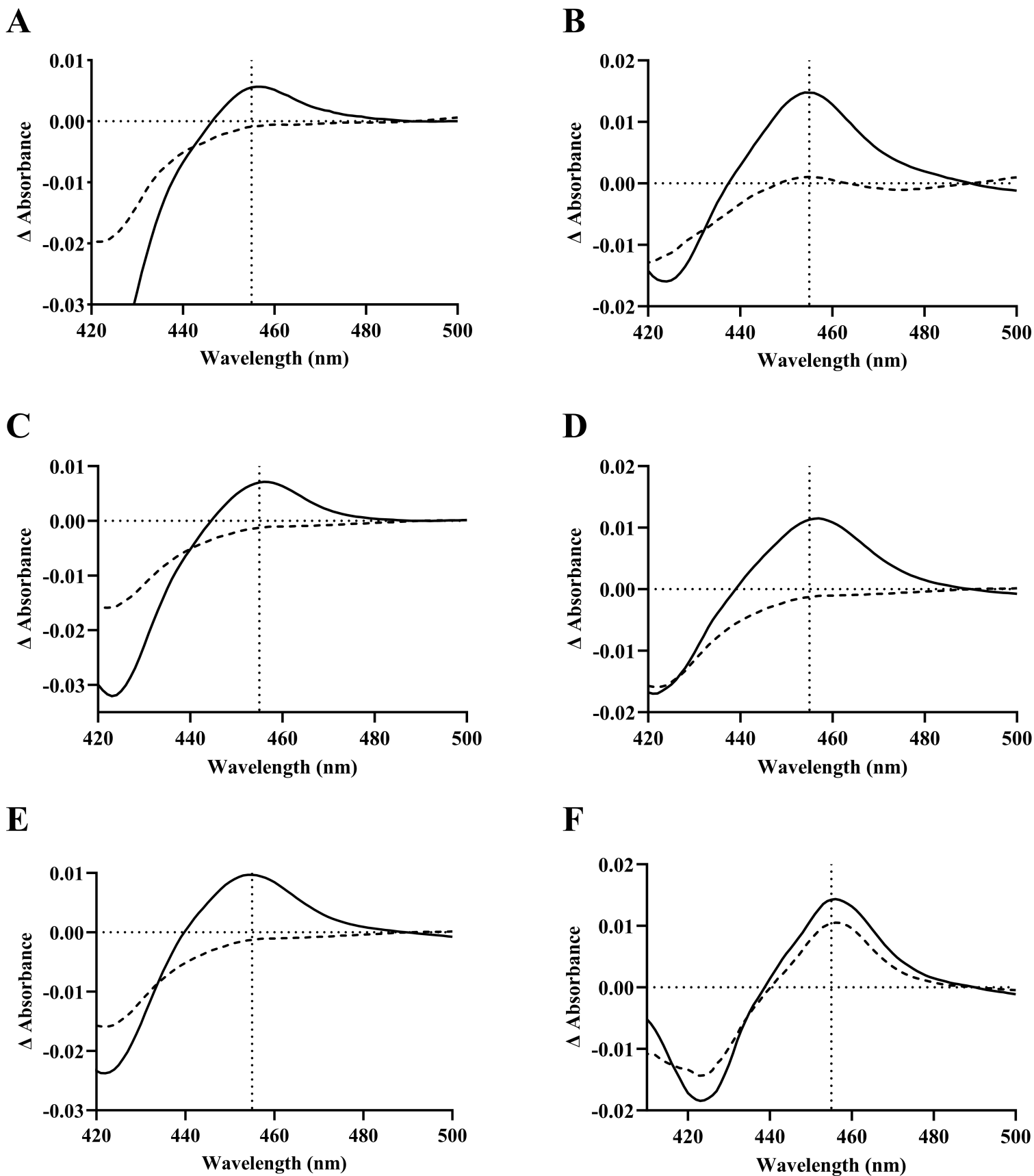


Figure 3

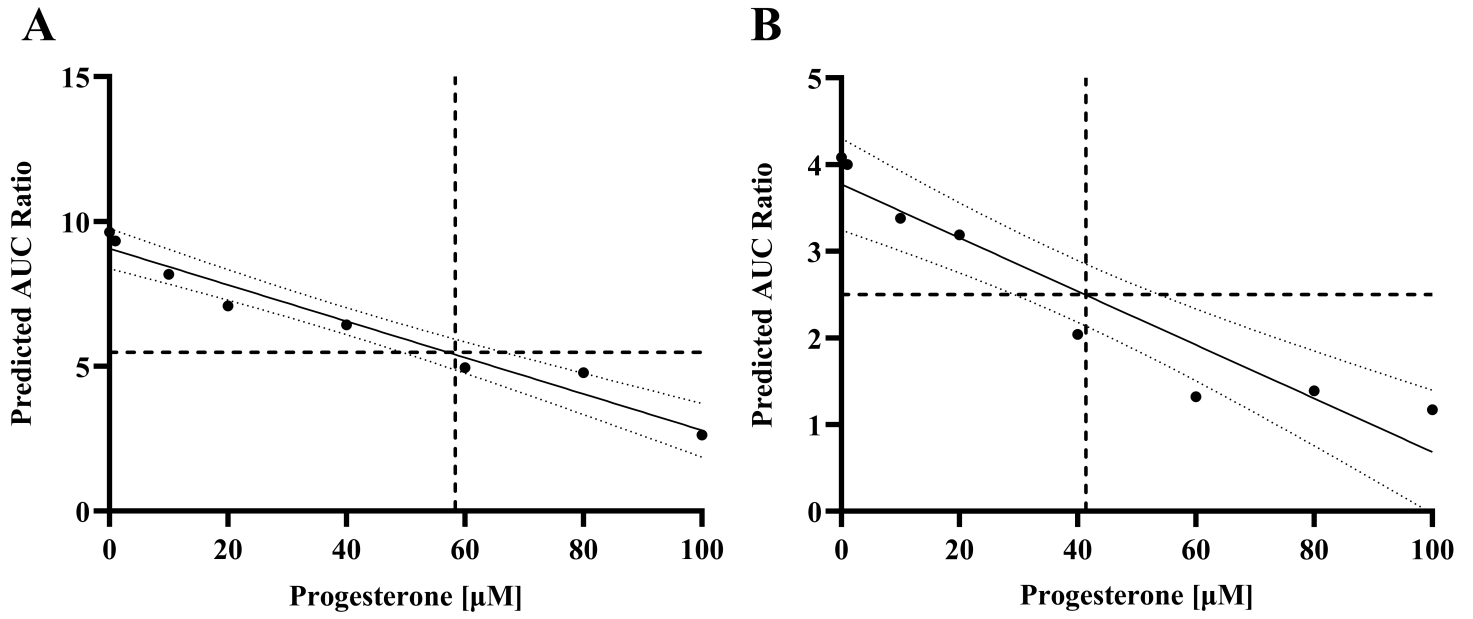


Figure 4